Egyptian Journal of Radiology and Nuclear Medicine

RESEARCH

Open Access

Skull base "intrinsic" bony mass lesions: conventional, diffusion and perfusion imaging with a proposed imaging approach

Lamya Eissa[1*] and Rim Aly Bastawi[1]

Abstract

Background and purpose Imaging with conventional MRI plays a pivotal role in characterization of skull base bone-intrinsic lesions, yet some lesions are very challenging. The purpose of this study is to evaluate the role of diffusion and perfusion by T2* dynamic susceptibility contrast (DSC) in characterization of such lesions.

Results Lesions showed mostly correlated with approach: *Chordomas* had low perfusion and intermediate to high perfusion, while *chondrosarcoma* had ADC value > $1.6 \times 10^{-3}/cm^2$ and more perfused. *Metastases* had variable ADC values usually intermediate with high perfusion. *Plasmacytomas* had similar features yet with characteristic conventional morphology and single number. *Lymphoma* (primary bony) had high perfusion and lowest diffusion ADC (= 04–$0.7 \times 10^{-3}/cm^2$). *Giant cell tumors* and hemangiopericytomas had lowest perfusion.

Conclusion The proposed imaging approach showed very good results and high accuracy in differentiation of skull base bony lesions.

Keywords MRI, Skull base, Perfusion, Diffusion, DSC

Background

Skull base osseous masses are growths that developing in bones at skull base. These masses can be benign or malignant and can arise from various structures such as skull bones, nerves, vessels, or soft tissues. Imaging plays a crucial role in diagnosing and characterizing these masses. Being rare and nearly rarest of head and neck tumors, making a detrimental diagnosis a difficult task. CT provides details of bones of skull base. They can accurately show the size, shape, and extent of osseous masses and detect erosions and calcifications [1–3]. Magnetic resonance imaging (MRI) offers excellent soft tissue contrast and is valuable for assessing relations of osseous lesions with adjacent structures like nerves, vessels, and brain. MR is helpful for identifying any compression or invasion of these structures [2, 4–6]. Also, it helps differentiation of a lesion being an "intrinsic" to bone of skull base or being an extension from "neighborhood"; a step, which means nearly half job done!

MR has been widely adopted as a highly efficient modality in oncologic imaging. It is highly effective for diagnosing bone tumors and has some advantages over other imaging techniques, especially in characterization of soft tissue lesions. It has an important role in staging, planning treatment and follow-up visits of patients with bone tumors, and it is currently evolving with musculoskeletal tumors, either intrinsic bony or soft tissue tumors in last decade with more advanced technical tools [2, 7–11].

The major role of "conventional" MRI is the prime diagnosis of musculoskeletal tumors and mapping their topography. However, very often, conventional MR cannot determine if tumor is benign or malignant; hence,

*Correspondence:
Lamya Eissa
lamya.eissa@gmail.com
[1] Radiology Department, Alexandria Faculty of Medicine, Alexandria 21131, Egypt

kinetic and functional studies were tested to estimate physiologic properties of lesions. MR perfusion involves injection of contrast (usually gadolinium), followed by acquisition of MR images to capture passage of contrast through tissues. Perfusion provides information about tissue vascularity, blood flow, and micro-vascular density (MVD). Various advanced MR techniques, including dynamic-contrast-enhanced (DCE-MRI) and arterial spin labeling (ALS), are nowadays used for assessment of tumors and tumor-like lesions. The T1-based DCE-MRI can depict microvascular and cellular environments of musculoskeletal tumors and tumor-like lesions, shifting from mere morphological assessment, and allowing functional assessment of lesions, since it can be used to evaluate the complex inter-related processes in tumoral microenvironment including neo-angiogenesis and tissue hypoxia [12, 13]. Neo-angiogenesis, induced by growth factors released by tumor, is the pathophysiological basis of this technique. The neo-angiogenic vessels have peculiar characteristics of permeability, fragility and chaotic blood-flow patterns [14]. A common approach in the analysis of DCE-MR is drawing region of interest (ROI) and observance of how the average signal intensity in ROI varies with time, drawing curves and measuring perfusion parameters. Many investigators reported that DCE-MRI is helpful in differentiating between benign and malignant tumors and assessing neo-angiogenesis of tumors including skeletal tumors [15, 16].

Another MRI technique that provides additional role in oncological imaging is diffusion, which is based on studying molecular diffusion of intra-matrix molecules. The molecular diffusion is visualized via diffusion-weighted MR-DWI, where visible signal intensity is influenced by cell size, density and integrity [16]. This is a useful supplemental tool for distinguishing malignant from benign head and neck lesions including nearly all tissues (glandular, epithelial and nodal). Thus, diffusion has been widely incorporated in tissue characterization of skull base lesions, since they have definitely different matrices, which allows for tissue characterization between lesions [17, 18].

Methods

The ***purpose*** of our study was to propose a classification imaging approach derived proposed classification approach made by a long cumulative 18 years of extensive head and neck subspecialty work with MDT analysis of skull base lesions. We tried to utilize advanced imaging techniques by MRI diffusion and perfusion based on dynamic contrast-enhanced MR-T2*-Dynamic susceptibility contrast (DSC) with subjective qualitative analysis. (I) *Patients*: Our *retrospective* research aimed at patients who had been diagnosed with intrinsic skull base lesions, readily referred from "oncology," "oto-rhino-laryngology-ORL" and "Neurosurgery" wards, being referred to radiology department of our primary university hospital for MR imaging. The "Ethics Committee" of our medical institution approved our proposed protocol. Since it is retrospective study, *informed consent was not taken. Also we did not need to include CARE 2013 checklist for case reporting (No case reports in our already retrospective study).* We aimed to collect patients in archives from December 2018 to December 2023 including imaging data and final pathology results. *Inclusion criteria: (A) patients with skull base "intrinsic" masses.* "Intrinsic" means origin limited to intra-osseous content including: (1) notochord remnants including Chordomas and ecchordosis physaliphora, (2) chondrosis or chondral rests like chondrosarcoma, (3) vascular spaces like hemangiopericytoma, (4) hematopoietic system: leukemia, lymphoma, plasmacytoma and metastases, (b) Adult patients ≥ 18 years, (d) primary and recurrent lesions, *exclusion criteria* included (1) absolute contra-indications to MR, (2) Jugular fossa lesions or other foramina lesions, (3) lesions that appear as variants/developmental (e.g., fatty lesion of sphenoid), (4) petrous apex non-osseous (e.g., cholesteatoma or cholesterol granuloma), (5) age < 18 years, (6) "Neighborhood" masses like nasopharyngeal or sinus, (7) lesion with extensive dural tails (e.g., Meningioma), (8) definite cystic lesions (e.g., intradiplopic epidermoid), (9) fibro-osseous lesions as fibrous dysplasia, readily diagnosed by non-contrast CT, and (10) diffuse dysplastic diseases (e.g., Paget's disease).

MRI imaging

MR imaging was conducted on two 1.5 Tesla machine manufacturers system *"Achieva," Philips medical systems & "Siemens," Avanto, Germany*; both were using a dedicated 16-channel sense neuro-vascular head-and-neck coil: (*I) conventional* MRI protocol was tailored to cover skull base till upper neck. The standard acquisition parameters were: (a) scout images, (b) multiplanar-axial, coronal, and sagittal-T2-weighted, (c) fast-spin-echo (TR = 5001 ms, TE = 103 ms, NA-averages = 2, matrix = 256 × 256 mm; section thickness = 4.5 mm; and inter-slice gap = 3 mm), (d) axial T1-weighted (TR = 676 ms, TE = 8 ms, NA; number of averages = 3, section thickness = 3.5 mm, gap = 2 mm, matrix = 256 × 256 mm) (Fig. 1).

DWI-MRI

This was made by "Single shot turbo spin echo; "SS-TSE" sequence with these parameters (is used): axial 3-mm section thickness, FOV of 245 mm, and *B*-values of 0 and 1001 s/mm^2. ADC maps were generated from acquired images by ROIs manually drawn in DW images on solid

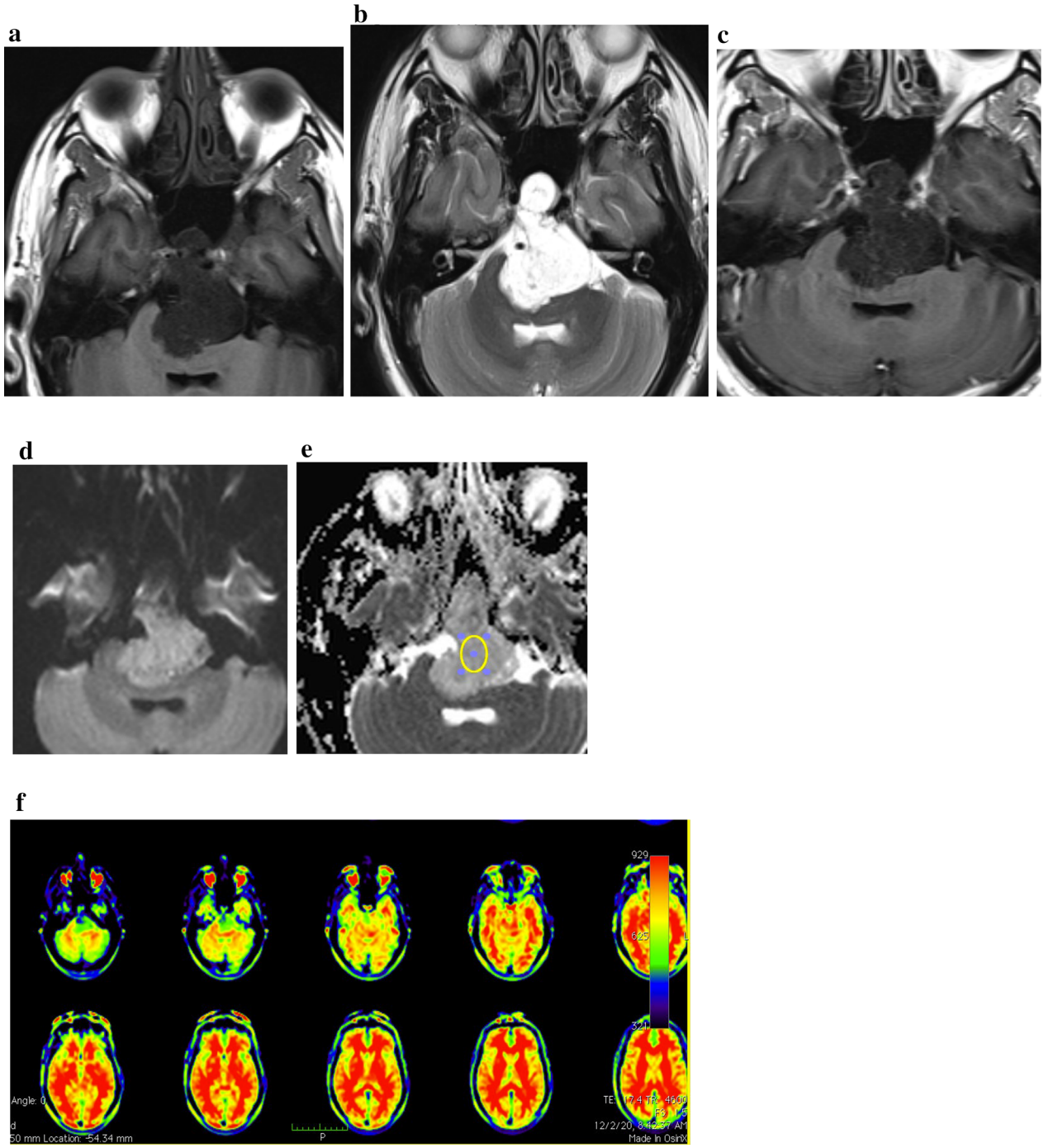

Fig. 1 A male patient 38 years old with pathology proven midline *clival chordoma*. Axial T1 image **a** shows homogenous T1 hypo-intense signal, **b** T2 homogenous very bright signal; CSF-like **c** T1 + GAD hypo-enhancement, **d** high signal at diffusion image with intermediate to high ADC value (ADC = 1.3–1.4 × 10^{-3} cm^2/s), shown in **e** and intermediate perfusion in color map scale in **f** showing areas of hypo-perfusion (blue). Quantitative analysis by a ROI shows low perfusion (= 183 mL/mg/min), less than normal parenchyma

portions of lesions, excluding non-solid regions, and ADC values were calculated using workstation software. Three ADCs were calculated, and the extracted mean ADC is used in statistical analysis. We used qualitative evaluation of the signal intensity in high b-1000 and described the lesion as hypointense (facilitated) or hyperintense (restricted) subjectively as compared to brain parenchyma (Fig. 2).

Dynamic T2* perfusion

Following diffusion, dynamic MRI sequence was obtained by injection of "Gadolinium; Gadopentate-dimeglumine" with a dose of 0.1 mmol/kg) and at a rate of 2 ml/s using power injector followed by 20 ml saline-flush. Sequential images were obtained through the lesion in axial plane, and with different time intervals at 30, 60, 90, 120, 150, 180, 250, and 300" s after injection. Then, conventional

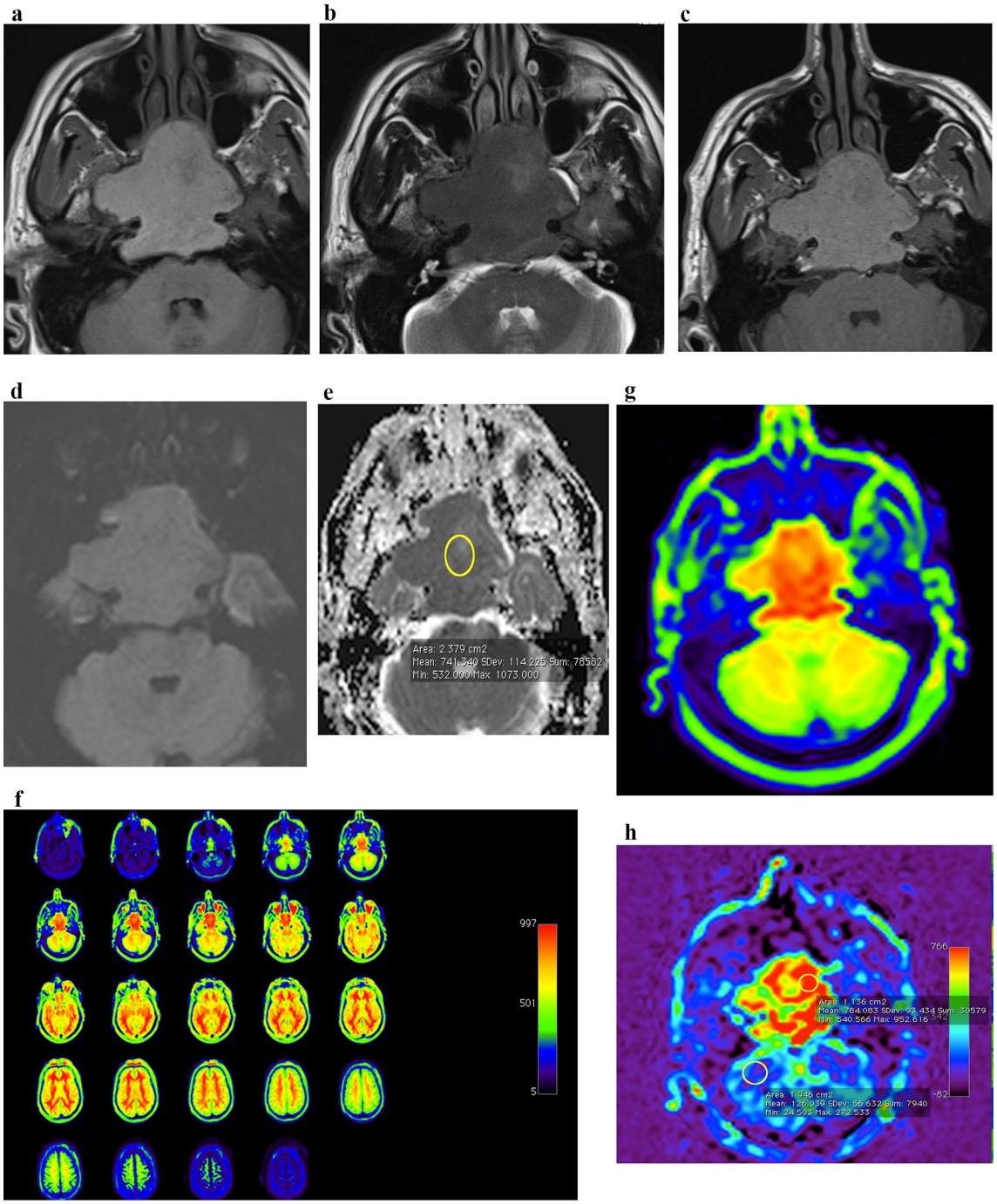

Fig. 2 A 57 years old female patient with proven clival *plasmacytoma*. Axial T1 image **a** shows T1-hyper-intense signal of compact cellularity and hemorrhages, corresponding to dark hypo-intense signal on Axial T2 image (**b**), with homogenous solid enhancement on axial T1 + GAD in (**c**). Axial diffusion shows iso-intense signal (**d**), with low ADC = 0.7×10^{-3} cm^2/s (**e**). Color map with scale (**f**) shows red color of high perfusion zoomed in (**g**). Quantitative analysis by ROIs **h** showed lesion having 7 times perfusion of the normal parenchyma (= 760 compared to 120 mL/mg/min)

post-contrast MRI fat-suppressed images are made in axial, sagittal and coronal planes, using same parameters as non-contrast axial T1 images, then subtraction is provided at axial images. Perfusion color maps images are interpreted on workstation (detailed below).

Post-processing and image analysis for DCE-MRI: The color maps are generated on dedicated software on *Mackbook pro (version 10.12.2; Early 2011)* after drawing ROI on solid enhancing portion; *Image Analysis*: A lesion was described regarding: (*1) site*: Midline clivus, para-midline clivus, petro-occipital fissure, petrous bone base or apex, mastoid bone, basi-occiput, (*2) size*: longest axis diameter in cms, *(3) Extensions*: Nasopharynx, sphenoid sinus, cavernous sinus, etc., *(4) Bony changes:* (a) geographic lytic destruction diagnosed by smooth bony destruction related to mass effect and pressure necrosis with wide zone of transition between normal and destroyed bone, (b) Permeative lytic destruction related to direct effect and enzymatic destruction, shown as irregular destruction and narrow zone of transition, (c) sclerotic with sclerotic lesion, *(5) matrix:* bone formation or hemorrhage by CT: (a) chondroid matrix: Intra-lesional ossified regular foci, (b) multiple osseous fragments, (c) solitary fragments, (d) calcifications, (e) hemorrhages, (f) sclerosis, *(6) Margins*: smooth or infiltrative, *(7) T1 signal:* compared to brain parenchyma as iso-, hypo- or hyper-intense), *(8) T2 signal: compared to brain parenchyma* as iso, hypo or hyper, bright if parallel to CSF signal) *(9) signal in high b-diffusion images* as hypo, iso, or hyper to brain signal, *(10) mean ADC* measured in = __x10^{-3} cm^2/s, *(11) enhancement*: "homogeneity" or "heterogeneity", and "degree of enhancement" as: (a) avid if parallel to dural venous sinus, (b) intermediate if below dural sinus, higher than parenchyma, (c) hypo-enhanced if near parenchyma, (d) non-enhanced shown by subtraction, (12) *perfusion* is graded in reference to brain parenchyma by color map. We used only *qualitative* method by color map scale so we can compare our results with researched different methods of perfusion other T2*-star perfusion. This is because our study is uniquely based on T2*based-DSC (*dynamic susceptibility contrast)* compared to quantitative parameters derived by T1-based DCE-MRI or permeability. *We graded perfusion* as follows: (a) blue = hypo-perfused, (b) green: low intermediate, (c) yellow: high intermediate, (d) red: high (Fig. 3).

Proposed diagnostic approach: is made by following criteria: (a) chordoma is diagnosed by a central or para-central mass with geographic pattern of bony destruction. T2 bright near CFS signal and high ADC > 1×10^{-3} cm^2/s and still < 1.6×10^{-3} cm^2/s, with intermediate to high perfusion and intermediate to avid contrast enhancement, (b) *chondrosarcoma* is diagnosed by central/paracentral, with geographic pattern of bony destruction, T2 bright near CFS signal and high ADC > 1.6×10^{-3} cm^2/s, with variable low-to-high perfusion, intermediate to avid enhancement, (c) *plasmacytoma* is diagnosed by centrally located, permeative lytic destructive mass, with T2 iso-to-hypo-intense signal, with low ADC < 1×10^{-3} cm^2/s, yet > 0.6×10^{-3} cm^2/s, high perfusion and intermediate to avid contrast enhancement, (d) *metastasis* diagnosed by history, multiplicity, permeative destruction, variable signal and enhancement pattern, intermediate ADC > 0.6×10^{-3} cm^2/s, & < 1.6×10^{-3} cm^2/s, and high perfusion, (e) *giant cell tumor* is suggested by a midline geographic lytic mass, with T1 hyper-intense signal (hemorrhages), variable T2 (hypo or hyper), low perfusion with variable yet high ADCs > 1×10^{-3} cm^2/s, (f) *lymphoma* diagnosed by a central destructive mass, T2 iso-to-low signal, *very low ADC* even < 0.6×10^{-3} cm^2/s and not > 1×10^{-3} cm^2/s. High perfusion and intermediate GAD contrast enhancement.

Statistical analysis of the data

The data were fed to the computer and analyzed using IBM-SPSS software package (version 23.0). Comparisons between groups for categorical variables were assessed using Chi-square test (Monte Carlo). *H*: Kruskal–Wallis test was used to compare between more than two categories for not normally distributed quantitative variables; sensitivity, specificity, PPV and NPV values were done and results were judged at the 5% level.

Results

Our study included 26 males and 24 females; median age was 48 (range = 18–82 years). The chordomas and chondrosarcomas made the largest number of cases; 24 lesions, 12 chordomas and 12 chondrosarcomas. This is followed by plasmacytoma ($n=9$), followed by metastases ($n=7$) distributed as one metastasis from breast cancer, two from lung cancer, one from prostate, one from RCC, one from papillary thyroid cancer, and last from colon cancer. This is followed by lymphoma ($n=5$) and giant cell tumor ($n=2$). One case of fibro-xanthoma, and another single case of hemangiopericytoma, with sarcomatoid changes. (Table 1) All lesions had been proven by stereotactic biopsy by skull base surgeon with endoscopic approach through nasal cavity and nasopharynx, apart from mastoid lesions approached by trans-canalicular (through EAC) approach and mastoid lesion approach by infra-zygomatic temporal approached (Fig. 4).

For locations: Most of the cases involved the midline clivus ($n=28$), followed by para-midline clivus ($n=9$) and right petro-occipital ($n=9$). Most of lesions showed no extension to neighborhood structures ($n=18$), while 9 showed extension into CPA, followed by nasopharynx

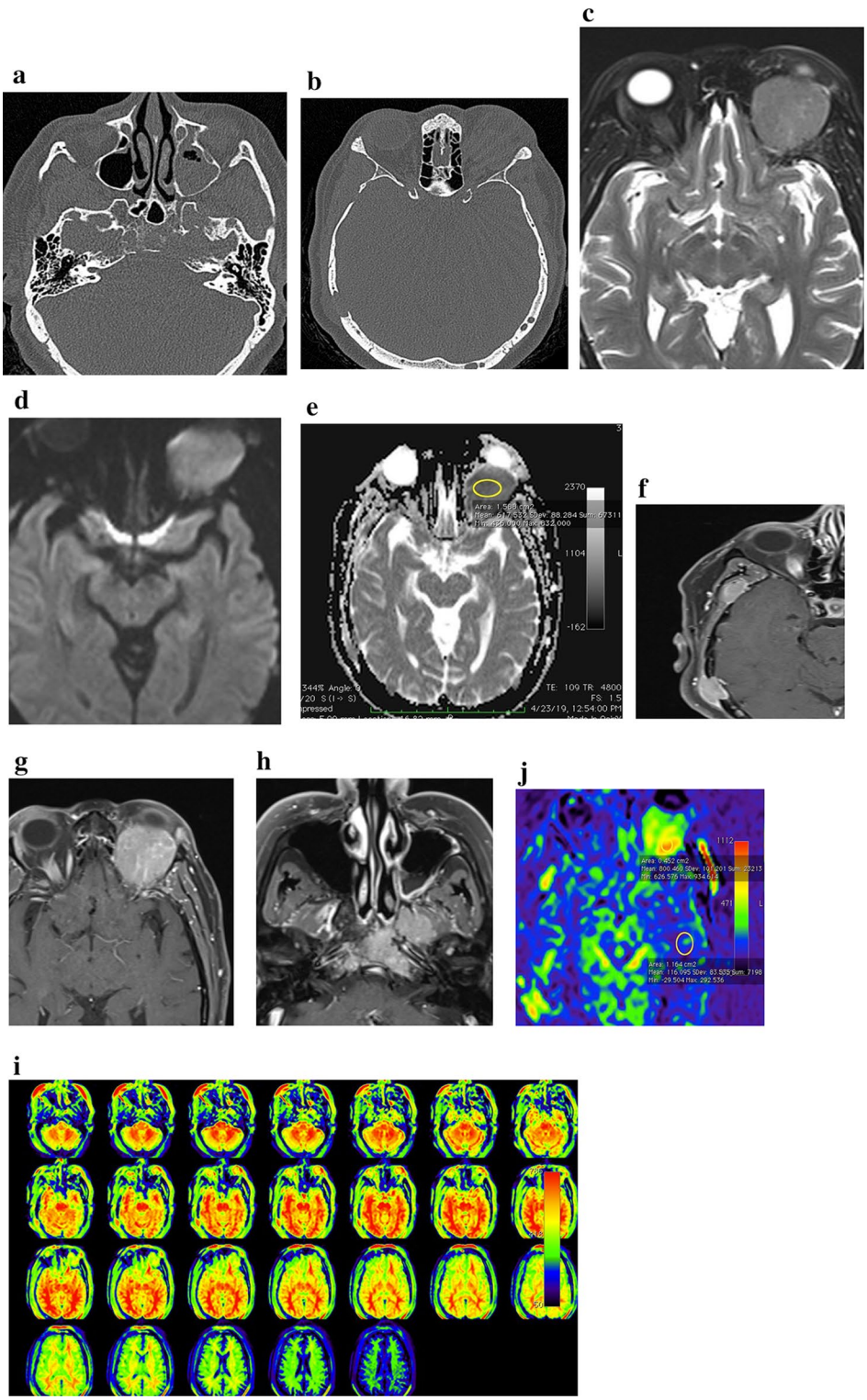

Fig. 3 A 53 years old female with multicenteric bony *lymphoma*. Non-contrast CT (**a**) and (**b**) revealed multiple lytic lesions of midline, anterior skull base, and calvarial bones. Axial T2 showed iso-intense orbital mass (**c**). Axial diffusion & ADC (**d** & **e**) showed iso-intense signal and very low ADC (= 0.5 x 10^{-3} cm^2/s) of middle skull base and larger orbital/anterior skull base mass (more obvious for illustration). Axial T1 GAD images in (**f**, **g**, **h**) revealed homogenous solid intermediate enhancement of all masses. Color map (**i**) hardly shows showing small lesions because of poor spatial resolution. Larger orbital mass shows intermediate to high perfusion with red areas of high perfusion zoomed in (**j**) with quantitative analysis by ROIs showing to have 8 times normal parenchyma (= 820 compared to 100 mL/mg/min).

($n=7$). This is followed by extension into sphenoid sinus ($n=6$), pre-pontine cistern ($n=6$), pre-medullary cistern ($n=5$) and Jugular foramen ($n=5$). (Summarized in Table 2).

Our study included 12 *chordomas*: T1 signal was hypo in 11 and iso in 1 case, T2 signal homogenously bright in 6, heterogeneous bright and intermediate in 5 and hyperintense in a single lesion. The mean size was 3.8 cm. Their mean ADC = 1.4×10^{-3} cm^2/s all lesions had well-defined margins. Five lesions had no bony matrix, 5 hade multiple fragments, a single lesion had a single fragment; a single lesion had dots of calcifications. Six cases showed lowest perfusion (Hypo-perfusion), while 6 showed low-to-intermediate perfusion. All lesions had permeative pattern of bony destruction.

The study enrolled 12 *chondrosarcomas*: T1 signal was hypo in 11, and iso in 1 case, 11 lesions showed homogenous T2 bright signal and a single lesion showed hyperintense to bright signal. The mean size was 3.8 cm. Their mean ADC = 1.9×10^{-3} cm^2/s (Range = $1.6–2.3\times10^{-3}$ cm^2/s), with eleven lesions had well-defined margins and a single lesion had infiltrative margins. Ten lesions had geographic pattern of bony destruction, and two had permeative. Only 4 had chondroid matrix, while 8 had no specific matrix. Six had low perfusion, and 6 others showed low- to intermediate perfusion (Fig. 5).

Five *lymphomas* were included. Four were iso-on T1 and 1 was hypo-intense. Four were T2-hypo-intense, while one was iso-intense. The mean size was 4.5 cm (range 2–6 cm). All lesions ($n=5$) were hyper-intense in diffusion images, with mean ADC = 0.6×10^{-3} cm^2/s, (Range = $0.4–0.7\times10^{-3}$ cm^2/s. Three lesions had well-defined margins, and two had infiltrative. The five lesions had permeative pattern of bony destruction. The five lesions had no specific matrix. The five lesions showed high perfusion.

We had seven *metastases* (*Primaries* are: two bronchogenic carcinoma, one RCC, one prostate, one colon, one breast, one papillary thyroidal cancer). Three showed hypo-intense signal and 4 showed T1 iso-intense signal. T2 signal was hypo in 2 lesions, iso-intense in two other lesions, hypo-to-iso-intense in one lesion and hyperintense in 2 more lesions. The mean size was 2 cm (range 1.5–4.5 cm). The mean ADC of lesions is 1×10^{-3} cm^2/s (Range = $0.8–1.3\times10^{-3}$ cm^2/s). Three had permeative pattern of bony destruction, 3 other had geographic pattern, and last one had sclerosis (prostate origin). Six lesions had non-specific matrix, and a single lesion had scleroses matrix. The 7 lesions had High perfusion.

We had 9 *Plasmacytomas*. 2 showed T1 hypo-intensity, 1 had hyper-intensity, and 6 lesions showed T1 iso-intense signal. The T2 signal was hypo-intense in 4 lesions and iso-intense in 4 lesions, as well as hypo-to-iso-intense in 2 more lesions. The largest size of our sample was a huge 12 cm plasmacytoma; the mean size was 4 cm (range 2.5–12 cm). Their mean ADC = 0.8×10^{-3} cm^2/s (Range = $0.7–1\times10^{-3}$ cm^2/s. Seven had well-defined margins, and two had infiltrative. Seven lesions had geographic pattern of bony destruction; two other had permeative pattern. All lesions had non-specific matrix. The whole 9 lesions had *High* perfusion.

The single lesion of *hemangiopericytoma* with *sarcomatoid changes* was wrongly diagnosed as plasmacytoma. This was a 4.5 cm midline clival destructive mass with T1 Iso and T2 iso-intense signal. It had a mean ADC = 0.8×10^{-3} cm^2/s. It shows geographic pattern of lytic destruction with no specific matrix. It shows heterogeneous avid post-GAD enhancement. It had low perfusion, which could have made the diagnosis of vascular lesion rather than cellular lesion as plasmacytoma or metastasis (Fig. 6).

The two case of *Giant cell tumor* had a T1 signal of iso- to hyper-intense signal; one of them showed heterogonous T2 iso to hyper, and the other heterogeneous hypo to iso-intense signal. They both showed homogenous avid post-contrast enhancement. The mean ADC = 1.6×10^{-3} cm^2/s (ADC range $1.5–1.6\times10^{-3}$ cm^2/s). Both lesions showed well-defined margins with geographic pattern of lytic destruction. They showed avid post-GAD enhancement yet both are hypo-perfused. Data of imaging parameters of different pathologies are summarized in Table 3. The measurements of accuracy of the proposed imaging approach including sensitivity and predictive values are mentioned in Table 5.

Table 1 Distribution of the studied cases according to site and extension

	No.	%
Final diagnosis		
Chordoma	12	24.0
Chondrosarcoma	12	24.0
Fibro-xanthoma	1	2.0
Giant cell tumor	2	4.0
Hemangiopericytoma with sarcomatous change	1	2.0
Inflammatory (Actinomycosis)	1	2.0
Lymphoma	5	10.0
Metastasis from breast cancer	1	2.0
Metastasis from colon cancer	1	2.0
Metastasis from lung cancer	2	4.0
Metastasis from papillary carcinoma thyroid	1	2.0
Metastasis from prostate cancer	1	2.0
Metastasis from RCC	1	2.0
Plasmacytoma	9	18.0

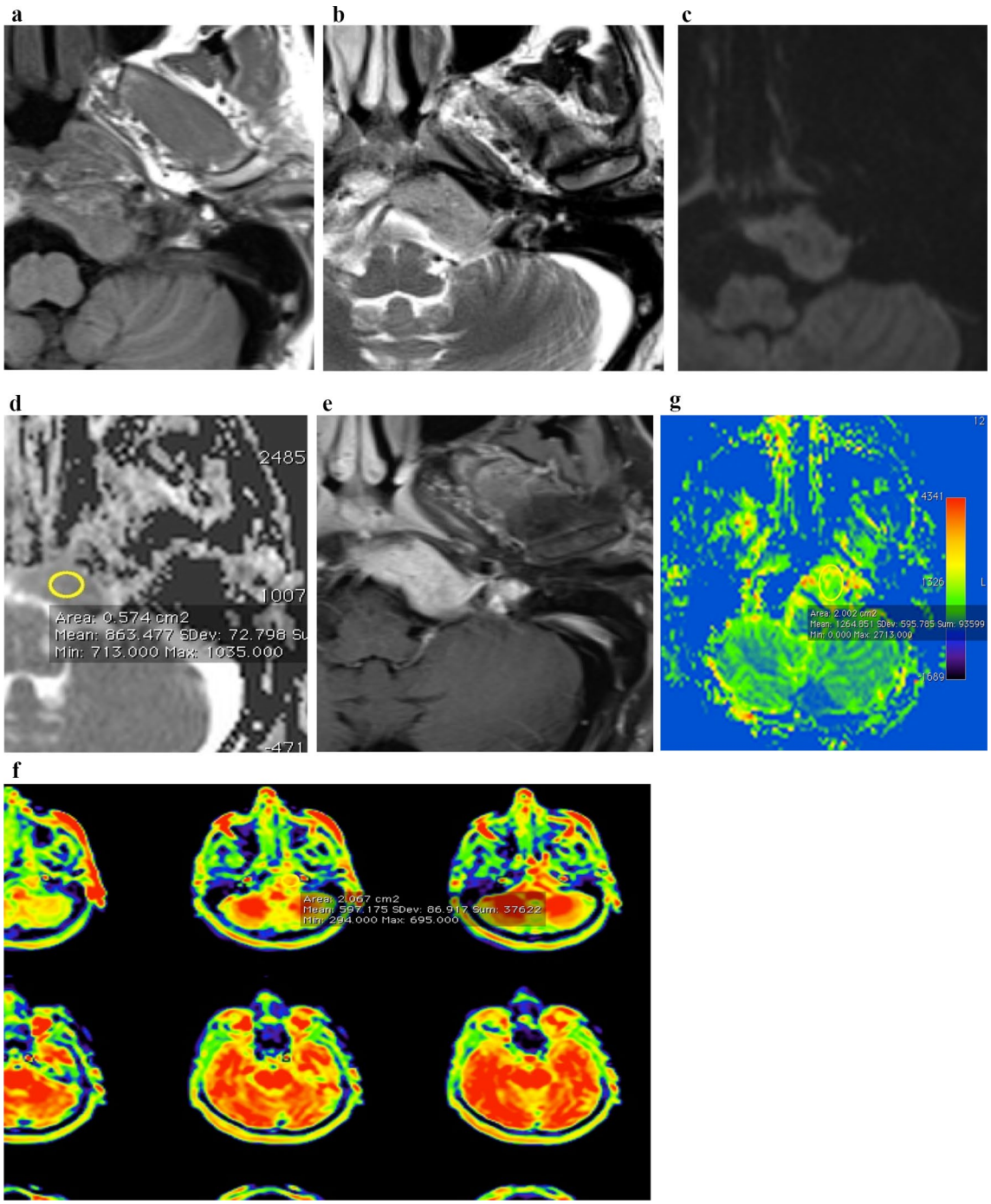

Fig. 4 A 53-year-old male patient with *falsely* diagnosed *plasmacytoma* versus metastasis and finally proven as a *hemangiopericytoma with sarcomatoid change*. Axial T1 and T2 images show iso-intense signal of left petrous bone mass (**a**, **b**). It is iso- to slightly hyper-intense in diffusion with ADC value ($=8.6\times10^{-3}$ cm^2/s) in (**c**, **d**) Axial T1 + GAD **e** revealed homogenous solid intermediate to avid enhancement. Color map **f** showed red spectrum of high perfusion. Additional quantitative analysis revealed very high perfusion of 1200 mL/mg/min, which is nearly 10 times normal parenchyma. Changes reflect those of round cell lesion which is matching with sarcomatoid change not underlying hemangiopericytoma, and rather than a metastasis

Table 2 Distribution of the studied cases according to Final diagnosis

	No.	%
Site		
Left occipital condyle	1	2.0
Left petro-occipital	3	6.0
Left petrous bone	2	4.0
Mastoid bone	1	2.0
Midline clivus	28	56.0
Right para-midline clivus	9	18.0
Petro-occipital bone	7	14.0
Left petrous apex	2	4.0
Right mastoid bone	2	4.0
Left para-midline clivus	1	2.0
Right petro-occipital	9	18.0
Right petrous apex	2	4.0
Extension		
None	9	18.0
Bilateral middle cranial fossae	1	2.0
Both cavernous sinuses	4	8.0
Right cavernous sinus	2	4.0
IAC	1	2.0
Jugular foramen	5	10.0
Left cavernous sinus	3	6.0
Left CPA	3	6.0
Left hypoglossal canal	1	2.0
Left orbit	1	2.0
Masticator space	1	2.0
Nasopharynx	7	14.0
Pre-medullary cistern	5	10.0
Pre-pontine cistern	6	12.0
Right CPA	8	16.0
Right EAC	1	2.0
Right TMJ	1	2.0
Sphenoid sinus	6	12.0

Discussion

Skull base tumors are relatively rare tumors as compared to remainder of head and neck lesions, especially the intrinsically bony ones. These include those arising from structures inherent to bone making skull base: Notochord remnants, cartilaginous remnants or synchondrosis, hematopoietic tissue and osteoid matrix. Diagnostic challenges arise from many factors: Rarity of lesions, overlap of imaging findings, being distinct from head and neck subspecialty experience with the need for musculoskeletal imaging knowledge. Moreover, differentiation of intrinsic from extrinsic lesions needs good anatomical knowledge of this complex region. Another challenge is difficulty of surgery or biopsy of these lesions, yet made more feasible by stereo-tactic endoscopic approaches nowadays. We aimed to test a proposed approach made by a long cumulative 18 years of extensive head and neck subspecialty work with Multidisciplinary Team (MDT) discussions of skull base lesions. We tried to utilize advanced imaging techniques by perfusion and diffusion, both depending upon variability of tissue matrices of different lesions (Table 4).

Chordomas are rare, slow-growing tumors typically arising from remnants of midline notochord. They are often located at skull base or along the spine. MR perfusion can provide valuable information about vascularization of chordomas, which is important for treatment planning [19, 20]. Our study included 12 chordomas: T2 signal was predominantly bright in 10, intermediate in one and hyper-intense in one lesion. This is in agreement with literature and its known pathologically matrix predominantly, made up of vacuolated phisallipherous cells, which also meanwhile explains for intermediate to high diffusivity as noted in our study, where with mean ADC of chordomas was $=1.4\times10^{-3}$ cm^2/s (Range $=1.2$–1.6×10^{-3} cm^2/s) (Table 5).

Chordomas are typically hypo-vascular tumors, meaning they have fewer blood vessels compared to other tumors. In chordomas, DCE-MRI typically shows low vascular perfusion and permeability characteristics due to the tumor's hypo-vascular nature. The contrast agent may take longer to wash into and out of tumor compared to surrounding tissues. Enhancement pattern in chordomas is often heterogeneous, reflecting variable vascularizations within the tumor. This low perfusion is consistent with the slow-growing and locally invasive characteristics of chordomas [20, 21].

Time–intensity curves (TICs) show signal intensity changes in tumor over time after contrast injection. Chordomas typically exhibit a slow gradual increase in signal (wash-in) then slow wash-out compared to more vascular tumors. T1-based-perfusion parameters—derived from DCE-MRI—in chordomas usually demonstrate low peak enhancement and slow wash-in and washout rates denoting low perfusion. The *k*-trans, which reflects vascular permeability, is low in chordomas, indicating low permeability. The "*ve*" (volume of extravascular extracellular space per unit volume of tissue) is low in chordomas due to their dense and cellular nature [22]. These data agreed with our results and favorably explain for low to intermediate perfusions in our study as six cases (50%) showed lowest perfusion "hypo-perfusion", while six showed "low-to-intermediate" perfusion [20, 21].

Chondrosarcoma is malignant tumor derived from cartilage rests. They can vary in aggressiveness, characterized by cartilage matrix production, and often

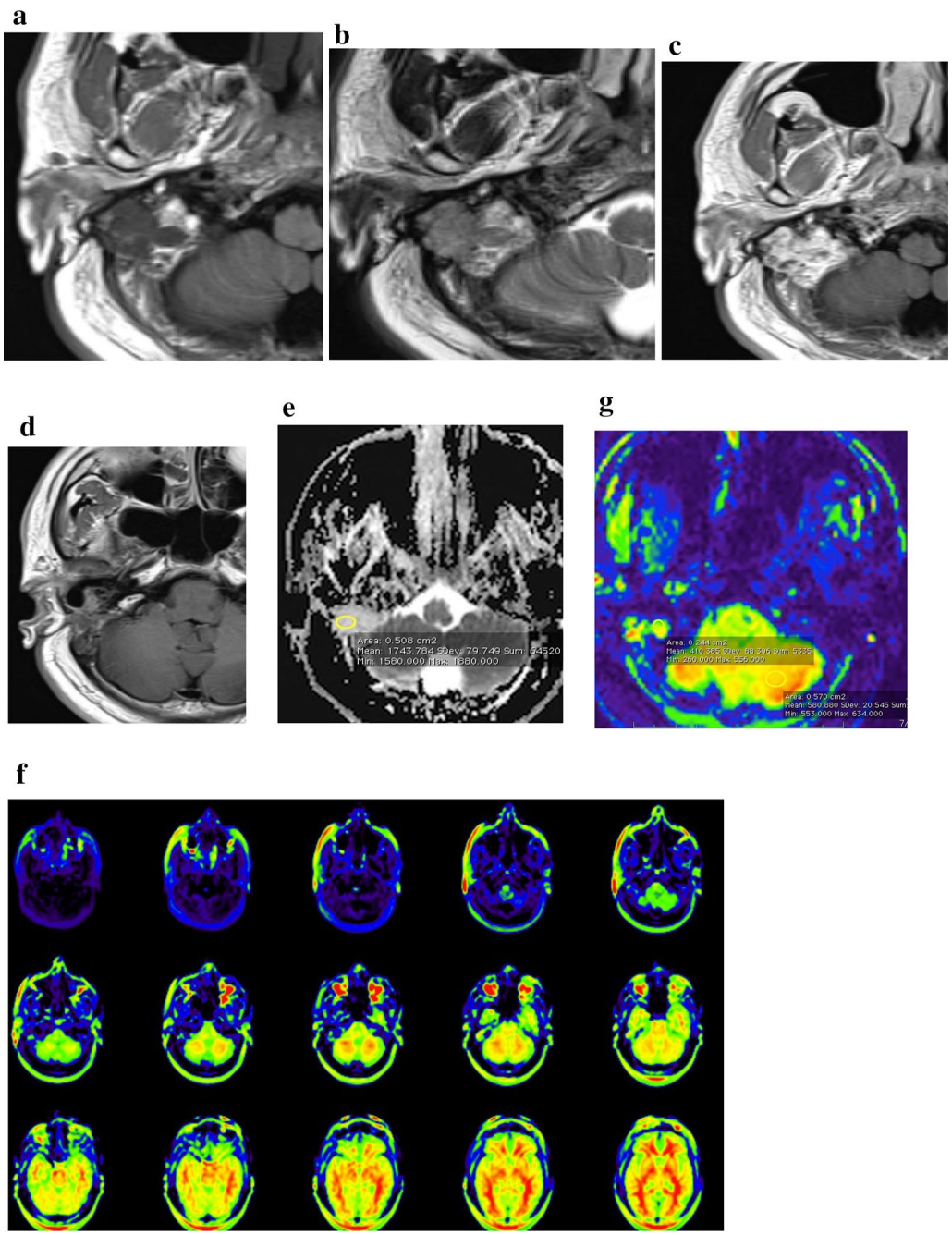

Fig. 5 A 42 years old male patient, presented right retro-auricular pain. Axial T1 and T2 (**a** & **b**) show hypoto iso-intense signal of mastoid bone well-defined lobulated lesion. Axial T1+GAD in (**c** & **d**) revealed homogenous solid hypo-to-intermediate enhancement, with extension into EAC. ADC map (**e**) shows facilitated diffusion with high ADC (= $1.7x10^{-3}$ cm^2/s). Color map in (**f**) shows hypo-to-intermediate perfusion, however zoomed in image (**g**) showed red areas of hyper-perfusion; still quantitative analysis showed hypo-perfusion (= 450 compared to normal parenchyma of 50 0mL/mg/min). Although features are all supporting a benign diagnosis, false preoperative diagnosis was made of metastasis because of hyper-perfused foci. A transcanalicular needle biopsy revealed a fibro-xanthoma. This is may be intrinsic bony or coming from dura

display varying degrees of vascularity and perfusion depending on their histologic grade. They typically show variegated enhancement-patterns. This variance is attributable to presence of variable components, such as hyaline cartilage, myxoid/cystic degeneration, or compact cellularity. This fact is well correlated with our findings, all showing hyper to bright T2 signals ($n = 12$). This also explained well for variability of mean

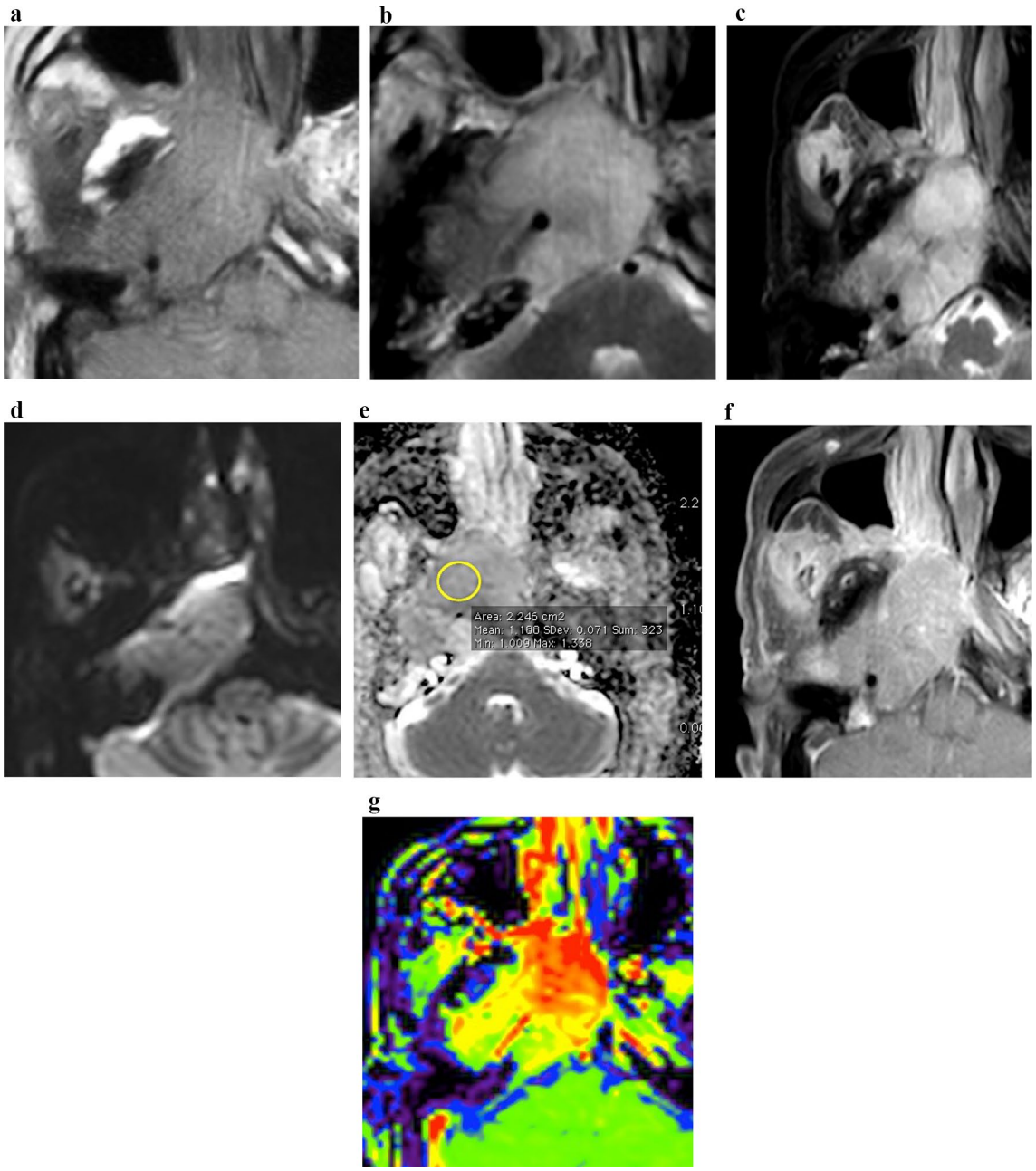

Fig. 6 A 48 years old male with old history of papillary thyroid carcinoma managed by total thyroidectomy with clear bed for ten years, and delayed *skull base metastases* epicentered on petro-clivus. Axial T1 (**a**) iso-intense signal of infiltrative mass at right petro-clivo-occipital bone, with hyper-intense signal in Axial T2 (**b**) pronounced in STIR (**c**), it is iso-to-slightly hyper-intense on diffusion (**d**) with intermediate ADC value ($=1.2\times10^{-3}$ cm^2/s) in (**e**), Axial T1 + GAD in (**f**) revealed slightly heterogeneous solid intermediate enhancement with a mass in masticator space. The color map **g** shows red color of very high perfusion. All imaging data are matching with malignant lesion (*A metastasis*)

ADC values of lesions, which was 1.9×10^{-3} cm^2/s (Range = $1.6–2.3\times10^{-3}$ cm^2/s), also being overall high. They also showed variable matrices: Only 4 had chondroid matrix, while 8 had no specific matrix [22, 23].

Also, it similarly explains for slightly variable perfusions: 6 had low perfusion and 6 others showed low to intermediate perfusion, while none of our proven low-grade chondrosarcomas had high perfusion. Reviewing literature, TICs in chondrosarcomas may vary depending on tumor histological grade; Higher-grade lesions tend to have more rapid intense enhancement,

Table 3 Imaging parameters, morphological and functional among different pathologies

Pathology	Final diagnosis																		Test of sig.	*p*
	Chordoma (*n* = 12)		Chondrosarcoma (*n* = 12)		Lymphoma (*n* = 5)		Metastasis (*n* = 7)		Plasmacytoma (*n* = 9)		Giant cell tumor (*n* = 2)		Hemangiopericytoma with sarcomatous change (*n* = 1)		Fibro-xanthoma (*n* = 1)		Inflammatory (Actinomycosis) (*n* = 1)			
	No.	%	No.	%	No.	%	No.	%	No.	%	No.	%	No.	%	No.	%	No.	%		
T1																				
Hypo	11	91.7	11	91.7	1	20.0	3	42.9	2	22.2	0	0.0	0	0.0	1	100.0	0	0.0	$\chi^2 = 51.201$*	$^{MC}p < 0.001$*
Hyper	0	0.0	0	0.0	0	0.0	0	0.0	1	11.1	0	0.0	0	0.0	0	0.0	1	50.0		
ISO	1	8.3	1	8.3	4	80.0	4	57.1	6	66.7	0	0.0	1	100	0	0.0	0	0.0		
ISO-to hyper	0	0.0	0	0.0	0	0.0	0	0.0	0	0.0	2	100	0	0.0	0	0.0	0	0.0		
T2																				
Hypo-intense	0	0.0	0	0.0	4	80.0	2	28.6	4	44.4	0	0.0	0	0.0	0	0.0	0	0.0		
Iso-intense	0	0.0	0	0.0	1	20.0	2	28.6	4	44.4	0	0.0	1	100.0	1	100.0	0	0.0		
Hypo-to-iso-intense	0	0.0	0	0.0	0	0.0	1	14.3	1	11.1	0	0.0	0	0.0	0	0.0	1	50.0		
Intermediate	1	8.3	0	0.0	0	0.0	0	0.0	0	0.0	0	0.0	0	0.0	0	0.0	0	0.0		
Hyper-intense	1	8.3	0	0.0	0	0.0	2	28.6	0	0.0	0	0.0	0	0.0	0	0.0	0	0.0		
Hyper-intense to bright	0	0.0	1	8.3	0	0.0	0	0.0	0	0.0	0	0.0	0	0.0	0	0.0	0	0.0		
Homoge-nous-bright	6	50.0	11	91.1	0	0.0	0	0.0	0	0.0	0	0.0	0	0.0	0	0.0	0	0.0		
Heterogene-ous iso-to-hyper	0	0.0	0	0.0	0	0.0	0	0.0	0	0.0	1	50.0	0	0.0	0	0.0	0	0.0		
Heterogene-ous-bright and interme-diate	4	33.3	0	0.0	0	0.0	0	0.0	0	0.0	0	0.0	0	0.0	0	0.0	0	0.0		
Heterogene-ous hypo-to-iso-intense	0	0.0	0	0.0	0	0.0	0	0.0	0	0.0	1	50.0	0	0.0	0	0.0	0	0.0		
Size in cm																				
Median (Min.–Max.)	3.8(1.5–6.5)		3.8(2.5–5.0)		4.5(2.0–6.0)		2.0(1.5–4.5)		4.0(2.5–12)		4.5(4.0–5.0)		4.5		2.5		2.5		H = 11.762	0.162
Mean ± SD	3.9 ± 1.4		3.9 ± 0.8		4.1 ± 1.6		2.4 ± 1.2		4.7 ± 2.9		4.5 ± 0.7									

χ^2, Chi square test; MC, Monte Carlo; *H*, Kruskal Wallis Test

*Statistically significant at $p \leq 0.05$

with a quick wash-in/out of contrast agent. Lower-grade chondrosarcomas show more gradual sustainable enhancement, as shown by T1-based DCE-parameters, as provided by Santos et al. [24], Bergh et al. [25], Katonis et al. [26], and De cornick et al. [27]. Similarly, the *k*-trans—a marker of tumoral vascular permeability—can vary according to tumor grade (Fig. 7).

Comparing chordomas and chondrosarcomas, with reviewing the literature, the apparent diffusion coefficient (ADC) values for either can vary, but generally, chordomas tend to have low ADC values, because vacuolated sheets of physallipherous cells are less diffuse than looser chondroid matrix which contains necrosis, cystic-myxoid degeneration, with consequent greater water diffusion [20, 21, 23]. Some studies suggested a cut-off-value of 1.6×10^{-3} cm^2/s, where lower values suggest chordomas and higher one suggest chondrosarcomas, nicely agreeing with our results and supported by Hayshida et al. [28].

Our study included five primary lymphomas; All ($n=5$) were quite restricted; with mean ADC of lesions is 0.6×10^{-3} cm^2/s. All lesions had high perfusion. This was in agreement with Barboriak [29], who reported strongly reduced ADC (0.64×10^{-3} mm^2/s), and Guo et al. [30], who stated that CNS lymphoma had lower ADC than other tumors. *However*, this was not matching with a study made by Kotb et al. [31], whose study included nine bony musculoskeletal lymphomas, showing higher mean ADCs ($=1.7\times10^{-3}$ mm^2/s; range $=1.02–1.9\times10^{-3}$ mm^2/s). They explained discrepancy of this by what was mentioned by Holscher et al. [32], who stated that signal attenuation on DWI is made by water molecules in extra-cellular space and by perfusion. Accordingly, Van Rijswijk et al. [33] explained overlapped ADC values by contribution of perfusion to the ADC values. Still, in agreement with ours, a study by Rodrigo et al. [34], on musculoskeletal soft tissue lymphomas: there were 7 cases, with a mean ADC value of $0.69\pm0.19\times10^{-3}$ mm^2/s. Still, generally speaking, skull base lymphomas often exhibit heterogeneous diffusion due to their complex histologic composition of cellularity and necrosis. This nicely explains for variable diffusion among lymphomas in literature and yet ours were restricted [23, 31, 35].

We had 7 metastases of different primaries as mentioned. Their mean ADC is 1×10^{-3} cm^2/s (range $=0.8–1.3$). Generally, malignant tumors show high cellularity, which is assumed to result in low ADC values in metastases. However, a study by Ota y et al. [23] suggested that mean ADC was not a significant differentiator between chordomas and metastases, which is assumed to complexity of internal structures and cellularity of each tumor group or from the heterogeneity of primary cancers of metastases [23].

Bone *metastases* often exhibit increased vascularity compared to normal bone tissue due to recruitment of new blood vessels to enhance tumor growth. Therefore, metastases exhibit higher perfusion values and more intense enhancement compared to benign lesions. The 7 lesions in our study had high perfusion by our qualitative analysis. However, Ota et al. [23] revealed clival metastases—which included a wide variety of primary cancer types—showed significantly higher *Vp* (quantitative perfusion) values than chondrosarcomas and chordomas. Studies, by Guan et al. [36], Morales et al. [37], Saha et al. [38], all showed that there were no significant differences in *Vp* (perfusion parameter) between vertebral hematologic malignancies and metastases. However, Ota Y's study showed higher *Vp* in vertebral metastasis from renal cancer (hyper-vascular tumor) than from prostate cancer (hypovascular tumor). This finding points *Vp* in bone metastases varies according to primary cancer type, which seems very logic reasoning. Nevertheless, Ota et al. [23], yet stated that, irrespective of the primary cancer type, they suggest that *Vp* remains a significant differentiator of metastases from primary bone lesions, such as chordomas or chondrosarcomas [23].

Our 9 plasmacytomas showed restricted diffusion; their mean ADC $=$ is 0.8×10^{-3} cm^2/s (Range $=0.7–$). In overall differentiation of musculoskeletal tumors, Rodrigo et al. [35] and Costa et al. [39] postulated that "small round cell" tumors (e.g., lymphomas and Plasmacytomas) showed more restricted diffusion than all other malignant soft tissue tumors, especially lymphoma (ADC as low as $<1.1\times10^{-3}$ cm^2/s) correlating with our study, while infections such as osteomyelitis showed restricted diffusion, with low ADCs. This was explained by Wong et al. [40] that purulent material and granulation tissues slow motion of water molecules. This was noticed with our case of action-mycosis, which had ADC $=1.1\times10^{-3}$ cm^2/s.

Plasmacytomas exhibit early and intense enhancement followed by a gradual washout of contrast agent on T1-based DCE-MR coping with hyper-perfusion. A study by Zhang et al. [41] confirmed that DCE-derived parameters of spinal plasmacytomas are significantly higher than those of spinal metastases [41]. This agreed with our observations; our nine lesions had high perfusion on DSC color map and intense GAD enhancement.

The two cases of *Giant cell tumor* had variable T1 and T2 signals reflecting hemorrhages of different chronological ages. Their mean ADC was 1.6×10^{-3} cm^2/s. Both lesions showed avid post-GAD enhancement yet both are hypo-perfused. In their largest series, by Chhabra et al. [42] being focused on GCTs of bones and

Table 4 Relation between final diagnosis and pathology "continue"

Pathology	Final diagnosis																		Test of sig.	*p*
	Chordoma (*n* = 12)		Chondrosarcoma (*n* = 12)		Lymphoma (*n* = 5)		Metastasis (*n* = 7)		Plasmacytoma (*n* = 9)		Giant cell tumor (*n* = 2)		Hemangiopericytoma with sarcomatous change (*n* = 1)		Fibro-xanthoma (*n* = 1)		Inflammatory (Actinomycosis) (*n* = 1)			
	No	%	No	%	No	%	No	%	No	%	No	%	No	%	No	%	No	%		
Diffusion																				
Hypo	0	0.0	0	0.0	4	80.0	4	57.1	1	11.1	1	50.0	0	0.0	0	0.0	0	0.0	$\chi^2 = 53.044$*	$^{MC}p < 0.001$*
ISO	0	0.0	0	0.0	1	20.0	1	14.3	7	77.8	0	0.0	1	100	1	100	1	100		
Hyper	12	100	12	100	0	0.0	2	28.6	1	11.1	1	50.0	0	0.0	0	0.0	0	0.0		
ADC																				
Median (Min.–Max.)	1.4(1.2–1.6)		1.9(1.6–2.3)		0.6(0.4–0.7)		1.0(0.8–1.3)		0.8(0.7–1.0)		1.6(1.5–1.6)		0.8		1.7		1.1		H = 45.392*	< 0.001*
Mean ± SD	1.4 ± 0.1		1.9 ± 0.2		0.6 ± 0.1		1.0 ± 0.2		0.8 ± 0.1		1.6 ± 0.1									
Margins																				
Well-defined	12	100	11	91.7	3	60.0	3	42.9	7	77.8	2	100	1	100	1	100	1	100	$\chi^2 = 12.530$	$^{MC}p = 0.064$
Infiltrative	0	0.0	1	8.3	2	40.0	4	57.1	2	22.2	0	0.0	0	0.0	0	0.0	0	0.0		
Bony changes																				
Geographic	12	100	10	83.3	0	0.0	3	42.9	7	77.8	2	100	1	100	1	100	1	100	$\chi^2 = 35.270$*	$^{MC}p = 0.001$*
Permeative	0	0.0	2	16.7	5	100	3	42.9	2	22.2	0	0.0	0	0.0	0	0.0	0	0.0		
Sclerosis	0	0.0	0	0.0	0	0.0	1	14.3	0	0.0	0	0.0	0	0.0	0	0.0	0	0.0		
Matrix bone																				
None	5	41.7	8	66.7	5	100	6	85.7	9	100	1	50.0	1	100	1	100	1	100	$\chi^2 = 76.832$*	$^{MC}p = 0.020$*
Single fragment	1	8.3	0	0.0	0	0.0	0	0.0	0	0.0	0	0.0	0	0.0	0	0.0	0	0.0		
Bone fragments	0	0.0	0	0.0	0	0.0	0	0.0	0	0.0	1	50.0	0	0.0	0	0.0	0	0.0		
Fragments	5	41.7	0	0.0	0	0.0	0	0.0	0	0.0	0	0.0	0	0.0	0	0.0	0	0.0		
Calcifications	1	8.3	0	0.0	0	0.0	0	0.0	0	0.0	0	0.0	0	0.0	0	0.0	0	0.0		
Chondroid	0	0.0	4	33.3	0	0.0	0	0.0	0	0.0	0	0.0	0	0.0	0	0.0	0	0.0		
Sclerosis	0	0.0	0	0.0	0	0.0	1	14.3	0	0.0	0	0.0	0	0.0	0	0.0	0	0.0		
Perfusion																				
Hypo	6	50.0	0	0.0	0	0.0	0	0.0	0	0.0	2	100	0	0.0	0	0.0	0	0.0	$\chi^2 = 85.309$*	$^{MC}p < 0.001$*
Low	0	0.0	6	50.0	0	0.0	0	0.0	0	0.0	0	0.0	0	0.0	0	0.0	1	50.0		
Low intermediate	6	50.0	6	50.0	0	0.0	0	0.0	0	0.0	0	0.0	0	0.0	0	0.0	0	0.0		
Intermediate to high	0	0.0	0	0.0	0	0.0	0	0.0	0	0.0	0	0.0	0	0.0	1	50.0	0	0.0		
High	0	0.0	0	0.0	5	100	7	100	9	100	0	0.0	1	100	0	0.0	0	0.0		

Table 4 (continued)

Pathology	Final diagnosis																		Test of sig.	*p*
	Chordoma (*n* = 12)		Chondrosarcoma (*n* = 12)		Lymphoma (*n* = 5)		Metastasis (*n* = 7)		Plasmacytoma (*n* = 9)		Giant cell tumor (*n* = 2)		Hemangiopericytoma with sarcomatous change (*n* = 1)		Fibro-xanthoma (*n* = 1)		Inflammatory (Actinomycosis) (*n* = 1)			
	No	%	No	%	No	%	No	%	No	%	No	%	No	%	No	%	No	%		
Enhancement homogeneity																				
Homogenous	10	83.3	8	66.7	5	100.0	7	100.0	8	88.9	1	50.0	1	100.0	1	100.0	0	0.0	$\chi^2 = 9.814$	$^{MC}p = 0.225$
Heterogeneous	2	16.7	4	33.3	0	0.0	0	0.0	1	11.1	1	50.0	0	0.0	0	0.0	1	100.0		
Enhancement degree																				
Hypo-enhancement	2	16.7	0	0.0	0	0.0	0	0.0	0	0.0	0	0.0	0	0.0	0	0.0	1	100.0	$\chi^2 = 66.281$*	$^{MC}p < 0.001$*
Low to intermediate	0	0.0	0	0.0	4	80.0	1	28.6	3	66.7	0	0.0	0	0.0	0	0.0	0	0.0		
Intermediate	4	33.3	1	8.3	1	20.0	4	42.9	6	66.7	0	0.0	0	0.0	0	0.0	0	0.0		
Intermediate to avid	3	25.0	2	16.7	0	0.0	1	14.3	0	0.0	0	0.0	1	100.0	0	0.0	0	0.0		
Avid	3	25.0	9	75.0	0	0.0	1	14.3	0	0.0	2	100.0	0	0.0	1	100.0	0	0.0		

χ^2, Chi-square test; MC, Monte Carlo; *H*, Kruskal–Wallis Test

*Statistically significant at $p \leq 0.05$

Table 5 Sensitivity, specificity, PPV and NPV for radiological diagnosis using proposed imaging approach

	Final diagnosis				Sensitivity	Specificity	PPV	NPV
	Negative (*n* = 0)		Positive (*n* = 50)					
	No.	%	No.	%				
Radiological diagnosis								
Negative	0	0.0	2	4.0	96.0	–	100.0	–
Positive	0	0.0	48	96.0				

NPV, negative predictive value; PPV, positive predictive value

tendon sheaths, they confirmed findings of previous case reports that overall ADCs of GCTs are quite low [42]. Also, mean ADC for all lesions was 1.0×10^{-3} mm^2/s in a study by Ashukyan et al. [43]. Generally speaking, it is believed that malignant hyper-cellular neoplasms demonstrate low ADCs, while benign neoplasms show higher ADCs. Our study is more matching with this hypothesis revealing relatively higher ADC values as mentioned [44]. However, it is yet difficult to presume an exact reason for low ADC values in GCTs, but some theories are plausible; presence of hemosiderin & thrombosed blood products and/or presence of hyper-cellular components. A study by Lobicher et al. [45] demonstrated a uniform perfusion pattern of GCT by dynamic MR, shown as

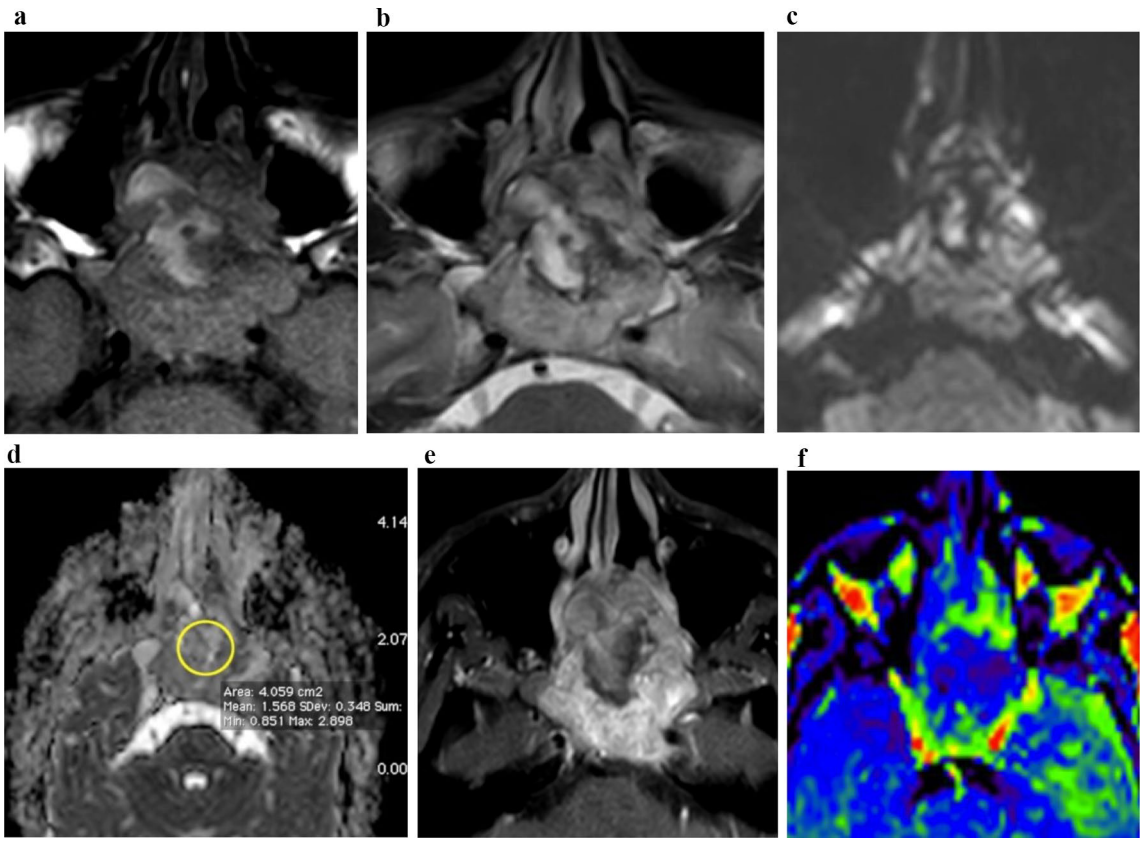

Fig. 7 A 32 years old male with proven *Giant cell tumor*. Axial T1 (**a**) lobulated midline clival mass with heterogeneous hyper-intensity, likely of old hemorrhages, corresponding to T2 hypo-intense signal (**b**), while diffusion (**c**) T2-blackout, with high ADC (= 1.5×10^{-3} cm^2/s) correlating with hypo-cellular nature (**d**). Axial T1 + GAD in (**e**) revealed peripheral solid avid enhancement expected at proliferative fibro-vascular growths in response to cumulative hemorrhages, with non-enhanced center. Color map **f** showed very hypo-perfusion at core of mass

steep slope followed by early rapid washout. This curve indicates hyper-perfusion while our two cases revealed hypo-perfusion; maybe due to variability in density of proliferative soft tissue and angiogenesis; though nearly whole literature agree with our study the avid delayed post-contrast GAD extra-cellular enhancement in relatively hypo-cellular abundant loose matrix.

Our study bears several *limitations*: *First*, it was conducted at a retrospective single institutional research and included a relatively small population. *Secondly*, adequate comparisons of perfusion parameters/values could not be achieved because we used another different perfusion techniques based on T2*-DSC susceptibility parameter which is different from all other literatures using more *quantitative* techniques (mostly DCE-MRI) and mainly musculoskeletal imaging outside head and neck regions, either osseous or soft tissue tumors. *Thirdly*, we included heterogeneous primary cancers in metastases, though this heterogeneous group could represent general population.

Conclusions

Interpreting diffusion-ADC and perfusion MRI findings (DSC) alongside conventional contrast-enhanced MRI can provide a comprehensive understanding of the tumor's tissue matrix thus helping in making differential diagnosis, especially between low grade and high-grade aggressive lesions. Our proposed approach is likely effective in a small scale. Recommended are further researches on wider scales and quantitative analysis, as diagnostic approach can help guide more focused stereotactic biopsy for most worrisome portion of tumor and aiding in treatment planning.

Abbreviations

MRI	Magnetic resonance imaging
GAD	Gadolinium
ADC	Apparent diffusion co-efficient
DSC	Dynamic susceptibility imaging
DCE	Dynamic contrast-enhanced MRI
DWI	Diffusion weighted imaging
MVD	Microvascular density
GCT	Giant cell tumor
TIC	Time–intensity curves
ASL	Arterial spine labeling
ROI	Region of interest
EAC	External auditory canal
MDT	Multi-disciplinary team

Acknowledgements

Not applicable.

Author contributions

LE gave the idea, provided the cases and final diagnoses, with detailed description of results; RB wrote the section of introduction and provided the whole references for introduction and discussion with making of figure legends. All authors read and approved the final manuscript.

Funding

This study had no funding from any resource.

Availability of data and materials

The datasets used and/or analyzed during the current study are available from the corresponding author on reasonable request.

Declarations

Ethics approval and consent to participate

All procedures followed were in accordance with the ethical standards of the responsible committee on human experimentation (Institutional Review Board *(IRB)"* of Alexandria General Hospital on December 14th, 2021; this is was updated in December 5th, 2023) and with the Helsinki Declaration of 1964 and later versions. Committee's reference number is unavailable (NOT applicable).

Consent for publication

No consent was obtained from the patients since it was a retrospective study. *CARE guidelines checklist of information* to include when writing a case report: Attached is a separate file of CARE-2013 check checklist (as requested by Journal); all as not applicable. Our study did not include any case report and even it is a retrospective study so an informed consent was not made.

Competing interests

The authors declare that they have no competing interests.

Received: 6 May 2024 Accepted: 27 August 2024
Published online: 20 September 2024

References

1. Jacobs MA, Wang X, Bluemke DA (2012) Musculoskeletal tumors: how to use anatomic, functional, and metabolic MR techniques 1. Radiology 265(2):340–356
2. Sharma G, Saran S, Saxena S, Goyal T (2022) Multiparametric evaluation of bone tumors utilising diffusion weighted imaging and dynamic contrast enhanced magnetic resonance imaging. J Clin Orthop Trauma 30:101899
3. Ab King AD (2007) Multimodality imaging of head and neck cancer. Cancer Imaging 7(special issue A):S37–S46
4. Ac Verstraete KL, Van der Woude HJ, Hogendoorn PCW, Deene YD, Kunnen M, Bloem JL (1996) Dynamic contrast-enhanced MR imaging of musculoskeletal tumors: basic principles and clinical applications. J Magn Reson Imaging 6:311–321
5. Choyke PL, Dwyer AJ, Knopp MV (2003) Functional tumor imaging with dynamic contrast-enhanced magnetic resonance imaging. Magn Reson Imaging 17:509–520
6. Dor Y, Porat R, Keshet E (2001) Vascular endothelial growth factor and vascular adjustments to perturbations in oxygen homeostasis. Am J Physiol Cell Physiol 280(6):1367–1374
7. Choyke PL, Dwyer AJ, Knopp MV (2003) Functional tumor imaging with dynamic contrast-enhanced magnetic. Reson Imaging 520:509–520
8. Wan L, Wu M, Sheth V, Shao H, Jang H, Bydder G, Du J (2019) Evaluation of cortical bone perfusion using dynamic contrast enhanced ultrashort echo time imaging: a feasibility study. Quant Imaging Med Surg 9(8):1383
9. El Backry M, Shady M, Mousa AE, Zaky MM (2015) Role of dynamic contrast enhanced MR perfusion in differentiation between benign and malignant tumors. Egypt J Radiol Nucl Med EJRN 46(3):715–726
10. Ae Hisatomi M, Yanagi Y, Konouchi H, Matsuzaki H, Takenobu T, Unetsubo T et al (2011) Diagnostic value of dynamic contrast-enhanced MRI for unilocular cystic-type ameloblastomas with homogeneously bright high signal intensity on T2-weighted or STIR MR images. Oral Oncol 47:147–152
11. Setiawati R, Novariyanto B, Rahardjo P, Mustokoweni S, Guglielmi G (2023) Characteristic of apparent diffusion coefficient and time intensity curve analysis of dynamic contrast enhanced MRI in osteosarcoma histopathologic subtypes. Int J Med Sci 20(2):163
12. Zampa V, Roselli G, Beltrami G (2010) MRI of bone tumors: advances in diagnosis and treatment assessment. Imaging Med 2(3):325–340
13. Botchu R (2021) Current progress and future trends in imaging of musculoskeletal bone tumours. J Clin Orthop Trauma 23(2):101622

14. Costa FM, Canella C, Gasparetto E (2011) Advanced magnetic resonance imaging techniques in the evaluation of musculoskeletal tumors. Radiol Clin N Am 49(6):1325–1358
15. Piludu F, Marzi S, Ravanelli M, Pellini R, Covello R, Terrenato I, Farina D, Campora R, Ferrazzoli V, Vidiri A (2021) MRI-based radiomics to differentiate between benign and malignant parotid tumors with external validation. Front Oncol 11:656918
16. Rezaeian A, Ostovari M, Hoseini-Ghahfarokhi M, Khanbabaei H (2022) Diffusion-weighted magnetic resonance imaging at 1.5 T for peripheral zone prostate cancer: the influence of the b-value combination on the diagnostic performance of apparent diffusion coefficient. Pol J Radiol 87:215–219
17. Norris CD, Quick SE, Parker JG, Koontz NA (2020) Diffusion MR imaging in the head and neck: principles and applications. Neuroimaging Clin N Am 30(3):261–282
18. Li S, Cheng J, Zhang Y, Zhang Z (2014) Differentiation of benign and malignant lesions of the tongue by using diffusion-weighted MRI at 3.0 T. Dentomaxillofac Radiol 44(7):0325
19. Srinivasan A, Galban CJ, Johnson TD, Chenevert TL, Ross BD, Mukherji SK (2010) Utility of the k-means clustering algorithm in differentiating apparent diffusion coefficient values of benign and malignant neck pathologies. AJNR Am J Neuroradiol 31(4):736–740
20. Koh DM, Collins DJ (2007) Diffusion-weighted MRI in the body: applications and challenges in oncology. Am J Roentgenol AJR 188(6):1622–1635
21. Soule E, Baig S, Fiester P, Holtzman A, Rutenberg M, Tavanaiepour D, Rao D (2021) Current management and image review of skull base chordoma: what the radiologist needs to know. J Clin Imaging Sci 11(46):1–11
22. Santos P, Peck KK, Arevalo-Perez J, Karimi S, Lis E, Yamada Y, Holodny AI, Lyo J (2017) T1-weighted dynamic contrast-enhanced MR perfusion imaging characterizes tumor response to radiation therapy in chordoma. AJNR Am J Neuroradiol 38(9):1–7
23. Ota Y, Liao E, Capizzano A, Baba A, Kurokawa R, Kurokawa M, Srinivasan A (2023) Differentiation of skull base chondrosarcomas, chordomas, and metastases: utility of DWI and dynamic contrast-enhanced perfusion MR imaging. Am J Neuroradiol AJNR 43(9):1325–1332
24. Santos P, Peck KK, Arevalo-Perez J (2017) T1-weighted dynamic contrast-enhanced MR perfusion imaging characterizes tumor response to radiation therapy in chordoma. AJNR Am J Neuroradiol 38:2210–2216
25. Bergh P, Kindblom LG, Gunterberg B (2000) Prognostic factors in chordoma of the sacrum and mobile spine: a study of 39 patients. Cancer 88:2122–2134
26. Katonis P, Alpantaki K, Michail K (2011) Spinal chondrosarcoma: a review. Sarcoma 2011:378957
27. De Coninck T, Jans L, Sys G (2013) Dynamic contrast-enhanced MR imaging for differentiation between enchondroma and chondrosarcoma. Eur Radiol 23:3140–3152
28. Hayashida Y, Hirai T, Yakushiji T, Katahira K, Shimomura O, Imuta M et al (2006) Evaluation of diffusion-weighted imaging for the differential diagnosis of poorly contrast-enhanced and T2-prolonged bone masses: initial experience. J Magn Reson Imaging 23(3):377–382
29. Barboriak DP (2003) New techniques for imaging brain tumors, including diffusion weighted and diffusion tensor MR. Oncologic imaging. In: American Rontegen Ray Society, annual meeting, San Diego, California, pp 11–24
30. Guo AC, Cummings TJ, Dash RC (2002) Lymphomas and high-grade astrocytomas: comparison of water diffusibility and histologic characteristics. Radiology 224:177–183
31. Kotb SZ, Sultan AA, Elhawary GM, Taman SE (2014) Value of diffusion weighted MRI in differentiating benign from malignant bony tumours and tumour-like lesions. Egypt J Radiol Nucl Med EJRN 45(2):467–476
32. Holscher HC, Hermans J, Nooy MA (1996) Can conventional radiographs be used to monitor the effect of neoadjuvant chemotherapy in patients with osteogenic sarcoma? Skelet Radiol 25:19–24
33. Van Rijswijk C, Kunz P, Hogendoorn PCW, Taminiau AHM, Doornbos J, Bloem JL (2002) Diffusion-weighted MRI in the characterization of soft-tissue tumors. J Magn Reson Imaging 15:302–307
34. Peckcvik Y, Kahya M, Kaya A (2015) Characterization of soft tissue tumors by diffusion-weighted imaging. Iran J Radiol 12(3):e15478
35. Rodrigo NR, Cabral D, Zenklusen MO, Bernocco F, Sanz R, Ward A (2022) Differentiation of benign and malignant musculoskeletal tumor lesions using diffusion-weighted magnetic resonance imaging. Rev Argent Radiol 86(1):3–22
36. Guan Y, Peck KK, Lyo J (2020) T1-weighted dynamic contrast-enhanced MRI to differentiate non-neoplastic and malignant vertebral body lesions in the spine. Radiology 297:382–389
37. Morales KA, Arevalo-Perez J, Peck KK (2018) Differentiating atypical hemangiomas and metastatic vertebral lesions: the role of T1-weighted dynamic contrast-enhanced MRI. AJNR Am J Neuroradiol 39:968–973
38. Saha A, Peck KK, Lis E (2014) Magnetic resonance perfusion characteristics of hypervascular renal and hypo-vascular prostate spinal metastases: clinical utilities and implications. Spine (Phila Pa 1976) 39:1433–1440
39. Costa FM, Ferreira S, Vianna EM (2011) Diffusion-weighted magnetic resonance imaging for the evaluation of musculoeskeletal tumors. Magn Reson Imaging Clin N Am 19:159–180
40. Wong AM, Zimmerman RA, Simon EM, Pollock AN, Bilaniuk LT (2004) Diffusion weighted MR imaging of subdural empyemas in children. AJNR Am J Neuroradiol 25:1016–1021
41. Zhang J, Chen Y, Zhang Y, Zhang E, Yu JH, Yuan H, Zhang Y, Su MY, Lang N (2020) Diagnosis of spinal lesions using perfusion parameters measured by DCE-MRI and metabolism parameters measured by PET/CT. Eur Spine J 29(5):1061–1070
42. Chhabra A, Ashikyan O, Slepicka C, Dettori N, Hwang H, Callan A et al (2019) Conventional MR and diffusion-weighted imaging of musculoskeletal soft tissue malignancy: correlation with histologic grading. Eur Radiol 29(8):4485–4494
43. Ashukyan O, Chalian M, Moore D, Xi Y, Pezeshk P, Chhabra A (2019) Evaluation of giant cell tumours by diffusion weighted imaging-fractional ADC analysis. Skelet Radiol 48(11):1765–1773
44. Ahlawat S, Fayad LM (2018) Diffusion weighted imaging demystified: the technique and potential clinical applications for soft tissue imaging. Skelet Radiol 47:313–328
45. Lobicher M, Bernd L, Schenk JP, Mädler U, Grenacher L, Kauffmann GW (2001) Characteristic perfusion pattern of osseous giant cell tumor in dynamic contrast-enhanced MRI. Ragiologie 41(7):577–582

Publisher's Note